Molecular Cell *21*, 337–347, February 3, 2006 ©2006 Elsevier Inc. DOI 10.1016/j.molcel.2006.01.011

The Molecular Basis of Filamin Binding to Integrins and Competition with Talin

Tiila Kiema,[1,5] Yatish Lad,[2,5] Pengju Jiang,[3] Camilla L. Oxley,[3] Massimiliano Baldassarre,[2] Kate L. Wegener,[3] Iain D. Campbell,[3] Jari Ylänne,[1,4,*] and David A. Calderwood[2,*]

[1] Biocenter Oulu
Department of Biochemistry
University of Oulu
FIN-90014 Oulu
Finland

[2] Department of Pharmacology and Interdepartmental Program in Vascular Biology and Transplantation
Yale University School of Medicine
New Haven, Connecticut 06520

[3] Department of Biochemistry
University of Oxford
Oxford OX1 3QU
United Kingdom

[4] Department of Biological and Environmental Science
University of Jyväskylä
FIN-14014 Jyväskylä
Finland

Summary

The ability of adhesion receptors to transmit biochemical signals and mechanical force across cell membranes depends on interactions with the actin cytoskeleton. Filamins are large, actin-crosslinking proteins that connect multiple transmembrane and signaling proteins to the cytoskeleton. Here, we describe the high-resolution structure of an interface between filamin A and an integrin adhesion receptor. When bound, the integrin β cytoplasmic tail forms an extended β strand that interacts with β strands C and D of the filamin immunoglobulin-like domain (IgFLN) 21. This interface is common to many integrins, and we suggest it is a prototype for other IgFLN domain interactions. Notably, the structurally defined filamin binding site overlaps with that of the integrin-regulator talin, and these proteins compete for binding to integrin tails, allowing integrin-filamin interactions to impact talin-dependent integrin activation. Phosphothreonine-mimicking mutations inhibit filamin, but not talin, binding, indicating that kinases may modulate this competition and provide additional means to control integrin functions.

Introduction

Cell adhesion, spreading, and migration involve a complex interplay between extracellular factors, cell-surface adhesion receptors, the actin cytoskeleton, and intracellular signaling networks (Ridley et al., 2003). Biochemical, cell biological, and genetic data point to important roles for actin crosslinking and scaffolding proteins from the filamin family in these processes (Cunningham et al., 1992; Stossel et al., 2001; van der Flier and Sonnenberg, 2001; Nagano et al., 2002; Feng and Walsh, 2004). Consistent with this, mutations in human filamin genes are associated with a wide range of developmental abnormalities and defective neuronal migration (Feng and Walsh, 2004).

In humans, three filamin isogenes have been identified of which filamin A (FLNa) is the most abundant and widely expressed (Stossel et al., 2001; van der Flier and Sonnenberg, 2001). Vertebrate filamins are homodimers of two 280 kDa subunits, and each subunit contains an N-terminal actin binding domain composed of two calponin homology domains followed by 24 tandem immunoglobulin-like domains (IgFLN1-24) that are interrupted by flexible hinge regions between domains 15 and 16 and 23 and 24 (Figure 1A). Dimerization through IgFLN24 results in a flexible parallel homodimer that can promote high-angle branching of actin filaments and is essential for stabilizing the orthogonal actin networks at the leading edge (Flanagan et al., 2001). In addition, the dimeric array of IgFLN domains acts as a scaffold for numerous transmembrane receptors and cytosolic signaling proteins (Stossel et al., 2001; Feng and Walsh, 2004). This permits assembly of complex networks linking transmembrane receptors with signaling proteins and the actin cytoskeleton. However, the molecular basis for these interactions—how specificity is determined and binding is regulated—is unknown.

We have previously examined the functional consequences of interactions between filamins and integrin adhesion receptors. By using both gain- and loss-of-function mutations, we found that binding of filamin to integrin β subunit cytoplasmic tails modulates cell migration (Calderwood et al., 2001). Integrins, heterodimers of α and β subunits, couple extracellular ligands to the cytoskeleton and intracellular signaling networks, permitting bidirectional transmission of biochemical signals and mechanical force across the plasma membrane (Hynes, 2002; Ridley et al., 2003). When bound to integrin β tails, FLNa is well placed to integrate integrin signaling and reorganization of the actin cytoskeleton.

Although there has been significant recent advances in understanding the structural basis of ligand binding by integrin extracellular domains (Springer and Wang, 2004), with the exception of the β3 integrin-talin interaction (Garcia-Alvarez et al., 2003) little is known about the structural basis of integrin β tail interactions with cytoskeletal, adaptor and signaling proteins. Here, we report the crystal structure of a filamin-integrin interface. The structure, along with NMR titration and mutagenesis, reveals the basis for integrin-FLNa interactions, identifies potential means for regulation of this interaction, and suggests a general mechanism for the binding of IgFLN domains to their partners.

Results

Mapping of the Integrin Binding Site on Filamin A

Our preliminary mapping of the integrin binding site took advantage of the susceptibility of filamin to proteolysis

*Correspondence: jylanne@cc.jyu.fi (J.Y.); david.calderwood@yale.edu (D.A.C.)

[5] These authors contributed equally to this work.

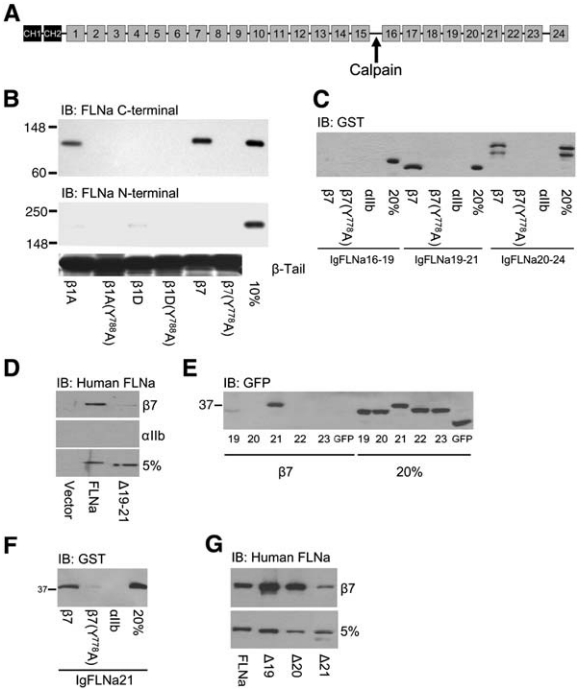

Figure 1. Localization of the Integrin Binding Site in FLNa

(A) Cartoon showing domain structure of filamin.

(B) N- and C-terminal fragments of filamin were generated by lysing platelets in the absence of protease inhibitors; their binding to beads coated with recombinant integrin tails was assessed in pull-down assays followed by immunoblotting. Bead loading with recombinant integrin tails was assessed by protein staining.

(C) Purified GST-IgFLNa16–19, 19–21, or 20–24 binding to integrin tails was assessed in pull-down assays.

(D) Pull-down assays were performed by using lysates from CHO cells transfected with empty vector, wild-type human FLNa, or domain deletion mutants. Bound proteins were detected by immunoblotting with anti-human FLNa antibodies.

(E) Binding of EGFP-fusion proteins of IgFLNa19, 20, 21, 22, and 23 expressed in CHO cells to β7-coated beads.

(F) Binding of purified GST-IgFLNa21 to integrin tails was assessed in pull-down assays.

(G) Binding of wild-type human FLNa or domain deletion mutants, expressed in CHO cells, to integrin β7 tails was assessed in pull-down assays. Lanes for 5%, 10%, or 20% represent corresponding percentage of the starting material in the binding assay.

by calpain (Stossel et al., 2001). Calpain rapidly cleaves FLNa between amino acids 1761 and 1762, generating fragments of approximately 190 kDa (up to IgFLNa15) and 100 kDa (IgFLNa16-24) (Figure 1A). To determine which region of filamin binds integrin β tails, endogenous platelet calpain was permitted to fully cleave filamin in platelet lysates, and the binding of fragments to recombinant model β tails was analyzed by affinity chromatography. β1A and β7 tails bound strongly to the ~100 kDa fragment, but not the ~190 kDa fragment, whereas the β1D tail exhibited negligible binding to either fragment (Figure 1B), consistent with its poor binding to intact filamin (Pfaff et al., 1998; Calderwood et al., 2001; van der Flier et al., 2002). Binding was abrogated by Tyr to Ala substitutions in the first NPxY motif of the β tails, which also inhibit binding of full-length filamin (Pfaff et al., 1998; Zent et al., 2000). Thus, analysis of calpain-generated filamin fragments localized the integrin binding site to IgFLNa16-24.

We next tested the ability of overlapping recombinant FLNa fragments spanning this region (IgFLNa16–19, 19–21, and 20–24) to bind β7 tails directly. IgFLNa19–21 and 20–24 bound strongly, consistent with previous reports (van der Flier et al., 2002; Travis et al., 2004), whereas IgFLNa16–19 showed negligible interaction (Figure 1C). Once again the binding was inhibited by Tyr to Ala substitution in the first NPxY motif of the β tail. IgFLNa19-21 fused to enhanced green fluorescent protein (EGFP) could also be pulled down from cell lysates by beads coated with recombinant β7 tails (data not shown), and β7 tails efficiently pulled down wild-type full-length FLNa, but FLNaΔ19–21 (lacking IgFLNa19–21) exhibited little β7 binding (Figure 1D). Thus, the major binding site for β7 integrin resides in IgFLNa19–21. Analysis of individual IgFLN domains expressed as EGFP-fusion proteins further localized a major binding site to IgFLNa21, with some weak interaction with IgFLNa19 (Figure 1E). Purified GST-IgFLNa21 also bound directly and specifically to β7 tails (Figure 1F), and, when the binding of increasing concentrations of GST-IgFLNa21 to the β7 tail was quantified by protein staining followed by scanning densitometry, curve fitting analysis indicated the apparent K_d of the β7 IgFLNa21 interaction to be 0.8 ± 0.2 μM (data not shown but see Figure 4B). Finally, human FLNaΔ21 (lacking IgFLNa21), but not FLNaΔ19 or FLNaΔ20, exhibited reduced binding to β7 tails (Figure 1G). Hence, IgFLNa21 contains a major binding site for integrin β7.

Crystal Structure of the Filamin-Integrin Complex

To reveal the molecular basis of the integrin-FLNa interaction, IgFLNa21 was crystallized together with a 31 residue peptide from the C terminus of the integrin β7 tail (L^{768}NWKQDSNPLYKSAITTTINPRFQEADSPTL^{798}), which spans the region previously implicated in filamin binding (Calderwood et al., 2001). The resulting crystals belonged to space group P2(1) and contained two molecules of IgFLNa21 in the asymmetric unit. The structure was solved by molecular replacement with a model derived from human IgFLNc24 (Pudas et al., 2005) and refined to 2.1 Å resolution to free R factor of 24.3% (crystallographic R factor 19.2%) (Table 1). In the crystal, two IgFLN domains form a noncrystallographic dimer through two integrin β7 peptides. The peptides form antiparallel β strands with each other and with the C strands of the IgFLN domain (Figure 2A). Both copies of IgFLNa21 are very similar to each other, and their interaction with the peptide is nearly identical (see Table S1 in the Supplemental Data available with this article online). The overall fold of human IgFLNa21 is very similar to IgFLNc24 (Pudas et al., 2005) and IgFLN4 and 5 from *Dictyostelium discoideum* filamin (McCoy et al., 1999; Popowicz et al., 2004) (Table S1); they form a distinct subfamily in the superfamily of E-set immunoglobulin-like β sandwich folds. Based on electron density and polypeptide mass determined by mass-spectrometry, both IgFLN domains in our structure have a glutathione molecule covalently bound to cysteine residue 2293 (Figure 2B). As discussed below, the glutathione is not required for integrin binding.

The interacting part of the β7 peptide consists of 13 residues spanning Pro^{776} to Pro^{788} (Figure 2B). This area is the stretch between two conserved NPxY/F

Table 1. Data Collection and Refinement Statistics

Data Collection		
	Fia1	Fia5
Space group	$P2_1$	$P2_1$
Cell dimensions		
a, *b*, *c* (Å)	42.5, 59.8, 52.3	42.0, 60.0, 51.6
α, β, γ (°)	90.0, 109.4, 90.0	90.0, 110.2, 90.0
Resolution (Å)	37.8–3.0 (3.10–3.00)[a]	37.7–2.10 (2.20–2.10)
R_{sym}	11.7 (25.2)	6.1 (35.5)
$I/\sigma I$	10.3 (6.0)	19.5 (6.9)
Completeness (%)	98.8 (99.2)	97.0 (96.7)
Redundancy	5.2 (5.2)	5.2 (5.2)
Refinement		
Resolution (Å)	37.80–3.00	37.7–2.10
Number reflections	4996	13748
R_{work}/R_{free}		19.2/24.3
Number atoms		
Protein		1564
Ligand/ion		52
Water		50
B-factors		
Protein		36.4
Ligand/ion		49.3
Water		35.3
Rms Deviations		
Bond lengths (Å)		0.014
Bond angles (°)		1.47

[a] Highest resolution shell is shown in parenthesis.

sequences found in all short integrin β tails. The rest of the peptide was not seen in the electron density. The β tail forms a β strand that lies anti-parallel to strand C of IgFLNa21 and extends the β sheet formed by the CFG strands. In addition to the main-chain hydrogen bonding required for the β strand conformation, there are many hydrophobic contacts in the interface (Figures 2B and 2C). Overall, the interaction surface on filamin covers 667 $Å^2$ of accessible surface area and has 64% nonpolar atoms and 36% polar atoms. On the β7 peptide, three nonpolar residues previously identified as important for filamin binding to integrin tails by mutagenesis (Zent et al., 2000; Calderwood et al., 2001) contribute most to the interface surface area; Tyr^{778}, Ile^{782}, and Ile^{786}. Tyr^{778} belongs to the first conserved NPxY motif and makes hydrophobic contacts with residues Pro^{2278}, Ser^{2279}, and Lys^{2280} in the C-D loop of IgFLNa21; its mutation to Ala inhibits binding of full-length filamin (Zent et al., 2000) and isolated IgFLNa21 (Figure 1F). Isoleucines 782 and 786 are important for strong binding of β7 integrin to filamin, and substitution by valine at these positions (as seen in the β1A tail) reduces filamin binding (Calderwood et al., 2001). Ile^{782} packs against IgFLNa21 strand D, making hydrophobic contacts with Ile^{2283} and Phe^{2285}, whereas Ile^{786} is located in a hydrophobic environment close to the loop between β strands B and C (Figures 2B and 2C). We note that in IgFLNa19, the residue corresponding to Phe^{2285} is Thr^{2094} (Figure S1), a fact that could explain the reduced integrin binding to IgFLNa19. Ala^{781}, immediately N-terminal to Ile^{782}, packs closely with residues in strand C, making hydrophobic contact with Ala^{2274}. Interestingly, Ala^{781} is conserved in the β1A, β2, β3, and β7 tails, which all bind filamin (Pfaff et al., 1998; Tadokoro et al., 2003; Sharma et al., 1995). In β1D, which binds poorly to filamin (Calderwood et al., 2001) (Figure 1B), this residue is changed to proline, a residue that would not easily fit in our structure.

Validation of the Interface by NMR and Mutagenesis

To analyze whether the interaction seen in the crystal also takes place in solution, the complex between the β7 peptide and IgFLNa21 was studied by NMR. Two forms of the domain were studied, one the same as in the X-ray studies, and the other with Cys^{2293} mutated to Ser. The spectra were assigned by using ^{15}N labeled samples, and ^{1}H-^{15}N HSQC spectra were monitored upon addition of β7 peptide. The shifts induced in both IgFLNa21 samples were very similar, but the Cys^{2293} to Ser mutant was better behaved in solution so the majority of the NMR data presented here were derived by using that sample. When the residues displaying significant chemical shift changes were mapped onto the crystal structure of IgFLNa21, they were concentrated in β strands C and D (Figures 2D and 2E). Because very similar effects were observed with the wild-type and Cys^{2293}Ser mutant domains, the glutathione does not have a significant effect on peptide binding.

To further validate the interface, Ala^{2272} and Ala^{2274} in strand C and Ile^{2283} in strand D of IgFLNa21 were substituted with the corresponding residues from IgFLNa22 or 23, which do not bind β7 tails (Figure 1E). Conservative IgFLNa23 substitutions (AA/ST or I/M) showed only minor effects on β7 tail binding, whereas AA/DK or I/C substitutions inhibited binding (Figure 3A). Together with the results from NMR titration (Figures 2D and 2E) and integrin mutagenesis (Figure 1F), these data show that the crystallographic β7-IgFLNa21 binding interface represents the interaction site in solution.

A General Model for Integrin-Filamin Interaction

β1A and β3 integrins also bind full-length filamin (Pfaff et al., 1998; Zent et al., 2000), and both bind IgFLNa21 (Figures 3B and 3C). Furthermore, tyrosine to alanine mutations in the first NPxY motif of β1A or β3 (corresponding to Tyr^{778} of β7) inhibit this interaction, and double valine to isoleucine substitutions in β1A, which increase binding to full-length filamin (Calderwood et al., 2001), also enhance binding to IgFLNa21 (data not shown). Likewise, mutations in the C or D strands of IgFLNa21 that inhibit binding of β7 tails also inhibit binding of β3 and β1A tails (Figures 3B and 3C). Finally, in NMR titration experiments, addition of β3 integrin peptides to IgFLNa21 induces chemical shift changes in β strands C and D (Figure 3D). Hence, NMR and mutagenesis indicate that IgFLNa21 is a general integrin binding site and that the structure of the β7-IgFLNa21 complex is representative of multiple integrin-filamin interactions.

The integrin β7 tail also binds to IgFLNa19 (Figure 1E). This interaction is direct and specific as β7 tails bind purified GST-IgFLNa19, but β7(Y^{778}A) and αIIb tails bind very poorly (Figure 3F). To investigate whether IgFLNa19 binds integrin in a similar fashion to IgFLNa21, we mutated the putative C and D strands of this domain. Mutations comparable to those that inhibited IgFLNa21 binding also inhibited IgFLNa19 binding (Figure 3G). NMR analysis revealed perturbation of residues at the CD face of IgFLNa19 during interaction with the β3 and β7 integrin tails (Figure 3E and data not shown), confirming the importance of this region for ligand binding. Thus,

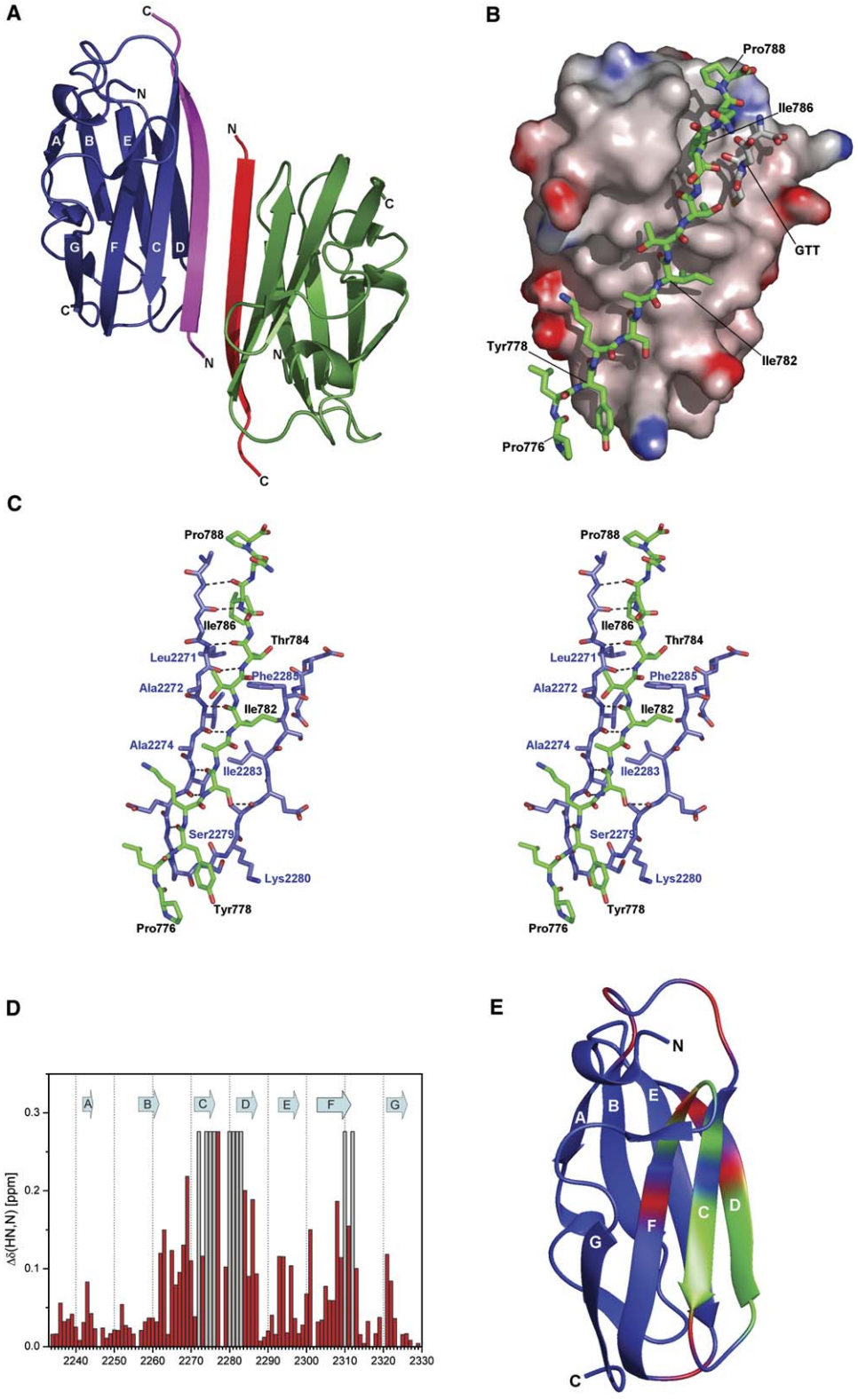

Figure 2. Crystal Structure and NMR Analysis of the IgFLNa21-Integrin β7 Cytoplasmic Tail Complex

(A) Ribbon diagram of the crystal asymmetric unit showing two filamin molecules (green and blue) interacting with two integrin β7 peptides (red and magenta).

(B) IgFLNa21-accessible surface colored according to electrostatic surface potential (red is negative charge and blue is positive charge). The β7 peptide is shown as green sticks on the filamin surface. The glutathione molecule covalently bound to the filamin Cys^{2293} is shown as gray sticks and is marked with GTT.

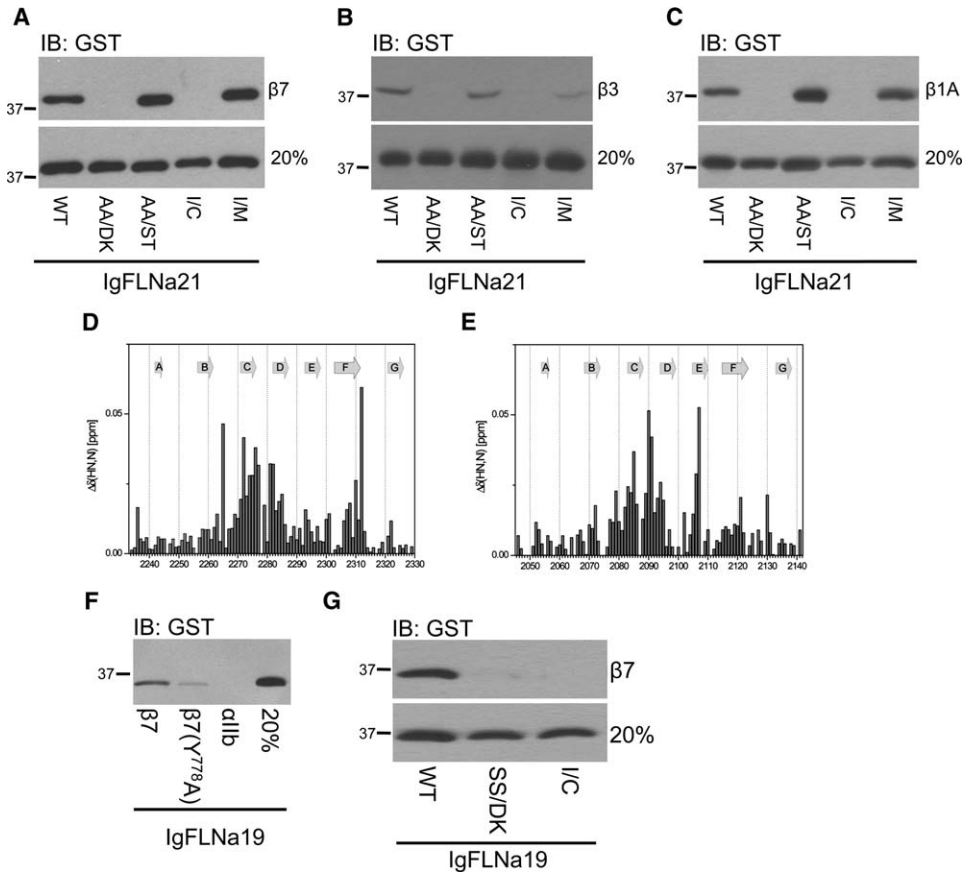

Figure 3. Integrins Bind to the CD Face of IgFLN Domains

(A) Binding of GST-IgFLNa21 containing mutations in strands C ($A^{2272}D$,$A^{2274}K$ or $A^{2272}S$,$A^{2274}T$) or D ($I^{2283}C$ or $I^{2283}M$) to recombinant β7 tails.
(B and C) Mutations in strands C or D of GST-IgFLNa21 inhibit binding to recombinant β3 and β1A tails.
(D and E) NMR chemical shift perturbation maps of the interaction of U-^{15}N-labeled IgFLNa21($C^{2293}S$) (D) or U-^{15}N-labeled IgFLNa19 (E) with the β3 tail peptide K^{738}WDTANNPLYKEATSTFTNITYRGT^{762} (an explanation of scales used is given in the legend to Figure 2D)
(F) Binding of purified wild-type GST-IgFLNa19 to recombinant β7 integrin tails was assessed in pull-down assays. Point mutations in the β7 tail inhibited IgFLNa19 binding.
(G) The effect of point mutations in the C ($S^{2081}D$,$S^{2083}K$) or D ($I^{2092}C$) strands of IgFLNa19 on binding to recombinant integrin tails was assessed in pull-down assays. Lanes labeled 20% represent 20% of the starting material in the binding assay.

the IgFLNa21-β7 complex provides a general model for integrin-filamin interactions.

The CD Face of IgFLN Domains Is a General Ligand Binding Face

Human filamins have multiple interaction partners (Stossel et al., 2001). We have now solved the structures of three different IgFLN domains in complex with peptide and protein ligands: the IgFLNa21-β7 integrin tail complex described here, IgFLNc24 with itself (homodimer) (Pudas et al., 2005), and IgFLNa17 with glycoprotein Ibα tail peptide (Nakamura et al., 2006). All three IgFLN domains adopt similar E-type Ig-like folds (Table S1) and bind ligand at the CD face of the β sandwich. Ligand binding involves extension of a β sheet by the interaction partner, and specificity is determined by H bonding and hydrophobic interactions. That this is a common ligand binding mode for IgFLN domains is further supported by NMR and mutational analysis of IgFLNa19-integrin β tail interactions (Figures 3E–3G). Thus, the CD face of IgFLN domains is likely to represent a common interaction surface for binding multiple ligands, and the IgFLNa21-β7 complex may provide a template for analysis of these interactions.

(C) Detailed stereo presentation of the integrin interaction with filamin. The integrin binding site, the CD-face (residues 2268–2287) of the filamin β sandwich, is shown as blue sticks. Hydrogen bonds between the peptide and filamin are shown as dashed lines.
(D) NMR chemical shift perturbation map of the interaction of U-^{15}N-labeled IgFLNa21($C^{2293}S$) with a β7 integrin tail peptide. $\Delta\delta$(HN,N) refers to the combined HN and N chemical shift changes, according to the equation $\Delta\delta(HN,N) = ((\Delta\delta_{HN}W_{HN})^2 + (\Delta\delta_N W_N)^2)^{1/2}$, where W_{HN} and W_N are weighting factors for the HN and N shifts, respectively ($W_{HN} = 1$, $W_N = 0.154$) (Ayed et al., 2001) and $\Delta\delta = \delta_{bound} - \delta_{free}$. Columns shown in pale gray indicate residues whose peaks experienced severe line broadening and could not be assigned in the bound state. The locations of the IgFLNa21 β strands are indicated.
(E) Chemical shifts from (D) mapped onto the crystal structure of IgFLNa21 from the IgFLNa21/β7 integrin complex. Residues with combined shift changes greater than 0.12 are indicated in red, whereas residues that underwent severe line broadening, and therefore were deemed to have also been strongly perturbed, are shown in green.

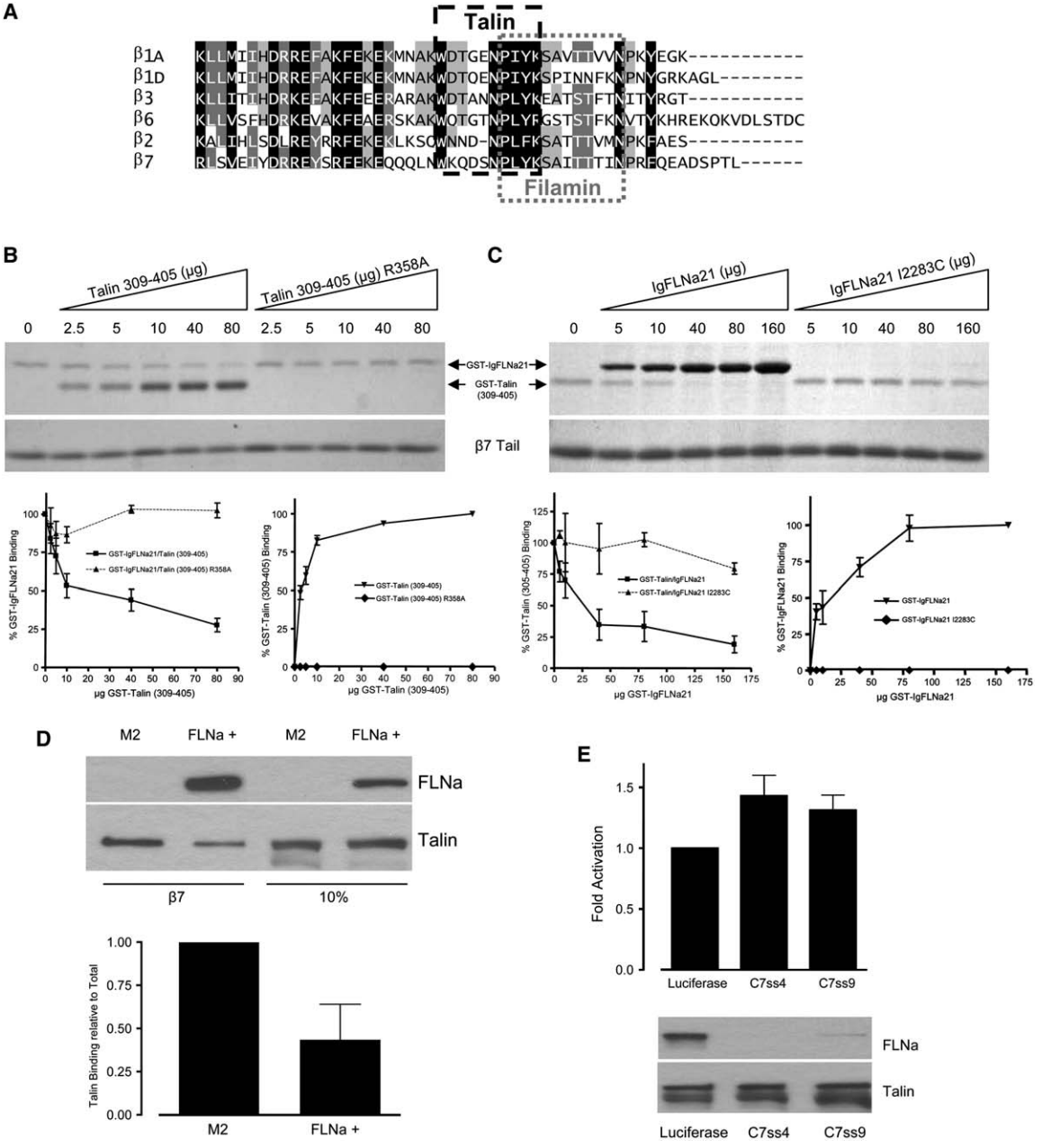

Figure 4. Filamin and Talin Compete for Binding Sites on Integrin

(A) Alignment of integrin β tail sequences showing the crystallographically defined talin (Garcia-Alvarez et al., 2003) and filamin binding sites.

(B) Increasing amounts of GST-talin (309–405) or the $R^{358}A$ mutant were mixed with 1 μg GST-IgFLNa21, and binding to recombinant β7 tails was assessed by protein staining of pull-down assays. Protein binding was quantified by densitometry and was expressed as a percentage of maximal binding in each experiment (error bars represent the mean ± SE; $n \geq 3$).

(C) Increasing amounts of GST-IgFLNa21 or GST-IgFLNa21($I^{2283}C$) were mixed with 1 μg GST-talin (309–405), and binding to recombinant β7 tails was assessed and quantified as in (B).

(D) Pull-down assays were performed with lysates from M2 or the FLNa reconstituted line ($FLNa^+$) cells with β7 tails. Bound proteins were detected by immunoblotting with anti-human FLNa or anti-talin antibodies. Lanes labeled as 10% represent the corresponding percentage of the starting material in the binding assay. Shown is the densitomeric analysis of talin binding relative to total talin levels (error bars represent mean ±SE; n = 3).

(E) Integrin activation was assessed by fibronectin fragment FN9-11 binding to NIH 3T3 FLNa knockdown lines (C7ss4 and C7ss9) by flow cytometry. Integrin activation is shown as fold activation relative to the Luciferase vector control cell line (error bars represent mean ± SE; $n \geq 7$). Total filamin and talin expression in these cells was determined by immunoblotting of cell lysates with anti-filamin and talin antibodies.

Filamin and Talin Crosscompete for Integrin Tail Binding

A large number of integrin β tail binding proteins have been identified (Liu et al., 2000), but, until now, the talin1-β3 integrin interaction was the only one for which high-resolution structural data was available (Garcia-Alvarez et al., 2003). β3 binds via a variant of the canonical PTB domain-ligand interaction; the first NPxY motif

forms a reverse turn, with the tyrosine pointing into a hydrophobic pocket, and residues upstream of this NPxY motif form a β strand that augments a β sheet in the talin PTB-like domain. Our work now shows that the talin binding and filamin binding regions of β tails overlap (Figure 4A), yet the tails adopt very different structures when bound to filamin or talin. For example, there is no NPxY reverse turn in the FLNa-β7 structure as the tyrosine N atom H bonds to Gly^{2277} in FLNa rather than to the OH group of the asparagine within the NPxY motif, as occurs when the integrin β tail is bound to talin (Garcia-Alvarez et al., 2003). This difference is consistent with a model in which flexible β tails rely on interactions with intracellular ligands to stabilize their structure (Ulmer et al., 2003). The overlapping binding sites suggested that filamin and talin would compete for binding to integrins. We therefore examined the effect of increasing amounts of GST-talin PTB domain (amino acids 309–405) on the binding of GST-IgFLNa21 to limiting quantities of integrin β7 tails. The integrin binding PTB-like domain of talin caused a dose-dependent inhibition of IgFLNa21 binding to recombinant β7 tails (Figure 4B). This inhibition was lost when the integrin binding defective mutant of the talin PTB domain, Arg^{358}Ala, (Tadokoro et al., 2003) was used (Figure 4B). Likewise, increasing amounts of GST-IgFLNa21, but not the nonintegrin binding mutant (Ile^{2283}Cys), inhibited binding of the talin PTB domain to integrin β tails (Figure 4C). The IC_{50} for inhibition by IgFLNa21 was calculated to be 1.0 ± 0.2 μM, in good agreement within error, with the 0.8 ± 0.2 μM apparent K_d calculated for IgFLNa21 binding to β7 tails. GST alone did not bind integrin tails and could not compete with IgFLNa21 or talin PTB domain (data not shown). Thus, the integrin binding domains of FLNa and talin can compete for binding to integrin β tails. Furthermore, recombinant integrin β7 tails bound more talin from lysates of FLNa-deficient M2 cells (Cunningham et al., 1992) than from lysates of M2 cells reexpressing FLNa, despite comparable levels of talin in each lysate (Figure 4D). This is consistent with competition between intact talin and FLNa proteins and suggests that competition may also occur in vivo.

The binding of talin to integrin β tails is a key step in the inside-out signaling that generates a high-affinity integrin (integrin activation) (Tadokoro et al., 2003). The mechanisms regulating integrin-talin interactions to modulate integrin activation are poorly understood (Calderwood, 2004), but, as shown above, our data indicate that competition with FLNa may provide one such mechanism. We therefore wished to test whether integrin activation was enhanced in filamin-deficient cells. Unfortunately, as assessed by the binding of soluble ligand (FN9–11; purified recombinant fibronectin type III repeats 9–11) or activation-specific anti-β1 integrin antibodies (9EG7 and HUTS-4), the β1 integrins expressed on the FLNa-deficient M2 melanoma cells are in a very low affinity state, thus, any further reduction by re-expression of FLNa could not be detected (data not shown). We therefore generated stable FLNa knockdown NIH 3T3 fibroblast lines and assessed the activation state of their α5β1 integrins by measuring the binding of FN9-11 in FACS-based assays. FN9-11 binding to NIH 3T3 cells was inhibited by EDTA and stimulated by

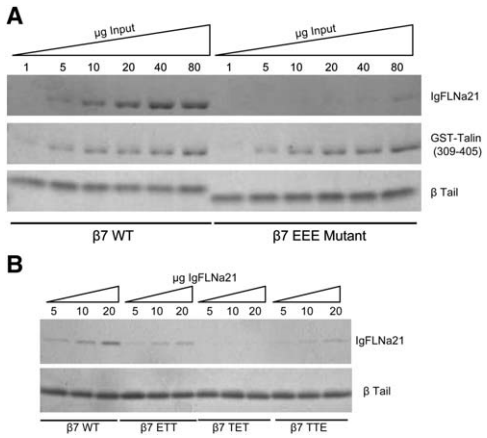

Figure 5. Regulation of Integrin-Filamin Interactions

Binding of increasing amounts of GST-IgFLNa21 or GST-talin (309–405) to recombinant β7 or β7 triple threonine mutant tails (A) or single β7 threonine mutants (B) was assessed by protein staining of pull-down assays.

the β1-activating antibody 9EG7 and Mn^{2+}, demonstrating its specificity (Tadokoro et al., 2003) (data not shown). To allow quantification of integrin activation, an activation index was calculated as the ratio of specific FN9-11 binding to maximal (9EG7-stimulated) specific FN9-11 binding (Zent et al., 2000; Tadokoro et al., 2003). Control cell lines expressing constructs that generate a shRNA-targeting luciferase had relatively active integrins (mean activation index of 0.55), but this was significantly increased in two separate FLNa knockdown lines despite all three lines expressing comparable levels of talin (Figure 4E). This increase in integrin activation is consistent with a loss of inhibition due to removal of competing FLNa in the FLNa knockdown cells, suggesting that at least in some circumstances, competition between filamin and talin can impact talin-dependent processes such as integrin activation.

Regulation of Integrin-Filamin Interactions

The filamin binding region of integrin β tails contains several potentially phosphorylatable residues (Fagerholm et al., 2004), and modification of these sites may impact filamin binding. β7 contains three threonine residues in this region; two (Thr^{783} and Thr^{785}) are exposed, whereas the middle one faces hydrophobic residues in IgFLNa21 strand D (Figures 2B and 2C). Introduction of three phospho-mimicking glutamate residues in place of these three threonine residues strongly inhibited the binding of GST-IgFLNa21 (Figure 5A). We therefore generated individual point mutations at each of the three threonine residues. This revealed that whereas phospho-mimicking mutations at either of the more exposed Thr^{783} and Thr^{785} residues impaired IgFLNa21 binding, modification of the buried Thr^{784} had the most pronounced effect on FLNa binding (Figure 5B). Therefore, phosphorylation of the β7 tail may regulate integrin-filamin interactions. Importantly, even in the triple phospho-mimicking mutation, talin binding to the β tail was not impaired (Figure 5A). Therefore, phosphorylation may provide a means to control FLNa binding and to modulate the competition between FLNa and talin.

Discussion

We have described the structural basis for interaction between the integrin family of cell adhesion receptors and FLNa, a major actin crosslinking protein and signaling scaffold with important roles in regulating cell migration. The structure reveals a link in the connection from extracellular matrices, via integrin and filamin, to the cortical actin cytoskeleton and adhesion-mediated signaling pathways. Our studies have identified a key integrin binding site in FLNa and the filamin binding site in integrin cytoplasmic tails. Our results help to explain previous mutagenesis data and identify additional mutations that may prove useful in further studies into the functional significance of integrin-filamin interactions. They also point to inhibition of FLNa binding by integrin threonine phosphorylation, allowing speculation on the signaling pathways that regulate integrin-filamin interactions. In addition, we have identified a general ligand binding site on IgFLN domains. Finally, we find that FLNa competes with talin, another large actin binding protein, for binding to integrin β tails and that this competition can impact talin-dependent processes such as integrin activation. Talin binding to integrin β tails is a key step in integrin activation and formation of the initial integrin-cytoskeletal links, and, so, the mechanisms regulating talin-integrin interactions are of considerable interest. Our finding that competition between filamin and talin provides one such mechanism has implications for our understanding of the assembly and remodeling of adhesions and their links to actin.

Mapping and Structure of the Integrin Binding Site on FLNa

We used proteolysis of endogenous protein, recombinant GFP-fusion proteins, purified GST-fusion proteins, and deletion of specific IgFLNa domains to localize the major integrin binding site in FLNa to IgFLN domains 19–21. Within this region, IgFLNa21 is the major integrin binding domain. However, we note that deletion of IgFLNa domains 19–21 consistently produces a more severe inhibition of integrin binding than deletion of IgFLNa21 alone, presumably because IgFLNa19 can partially compensate in the absence of IgFLNa21.

The crystal structure of IgFLNa21 bound to a β7 cytoplasmic tail peptide reveals that the FLNa domain adopts an immunoglobulin-type fold and that when bound to IgFLNa21, the integrin tail forms a β strand that interacts with the largely uncharged C-D face of the IgFLN β sandwich. The FLNa binding site lies between the conserved integrin NPxY motifs. This region was previously identified as important for filamin binding by mutagenesis and analysis of chimeric integrin β tails (Calderwood et al., 2001), and the three integrin residues identified as key for filamin binding (Tyr^{778}, Ile^{782}, and Ile^{786} in β7) (Zent et al., 2000; Calderwood et al., 2001) make major contacts at the IgFLNa21-β7 tail interface. With the exception of the β1D tail, which binds poorly to filamin, the sequence between the two NPxY motifs is relatively well conserved between integrins (Figure 4A), and NMR and mutagenesis suggest that the β7-FLNa interface is similar to that formed by other filamin binding integrins.

A General Interaction Surface on IgFLN Domains

At least 45 filamin binding proteins have been reported (Stossel et al., 2001; van der Flier and Sonnenberg, 2001; Feng and Walsh, 2004). The binding sites for most of these proteins map within IgFLN domains 14–24, and several include the integrin binding IgFLN21 domain. Crystallography of the IgFLNa21-β7 complex, the structures of IgFLNa17 bound to ligand (Nakamura et al., 2006) and the IgFLNc24 homodimer (Pudas et al., 2005), and NMR analysis and mutagenesis of IgFLNa19 lead us to suggest that the C-D face of the IgFLN domains is a general ligand binding interface. The interface involves extension of a β sheet, and the specificity of the interaction is determined by side chain interactions. We note that the residues on the IgFLNa21 C strand that interact with β7 are highly conserved in odd-numbered domains (17, 19, 21, and 23). In contrast, alignment of the D strands shows that the Phe^{2285}, which makes hydrophobic interactions with the β tail, is rather variable, changing to Thr in IgFLNa19 and Cys in IgFLNa17 and 23 (Figure S1). This variability may explain the specificity of tail recognition. The integrin-filamin structure reported here should therefore prove a useful template for mutagenic analysis of many other filamin interactions.

Regulation of Integrin-FLNa Interaction

The filamin binding region of integrin β tails contains several potentially phosphorylatable residues (Fagerholm et al., 2004), and modification of the three threonine residues within the filamin binding site of β7 inhibits filamin binding. Consistent with our crystal structure, the most severe effect is seen after modification of Thr^{784} that faces hydrophobic residues in IgFLNa21 strand D (Figures 2B and 2C).

There are two other potentially phosphorylatable residues within the FLNa binding regions of β7: Tyr^{778} in the first NPxY motif, which makes hydrophobic contacts with IgFLNa21 and is a potential substrate for Src family kinases (Fagerholm et al., 2004), and Ser^{780}, a PKC substrate (Fagerholm et al., 2004) that faces toward the D strand of IgFLNa21 and H bonds to Ala^{2281}. The effect of phosphorylation of these residues on filamin binding is unknown; however, it is likely that tyrosine phosphorylation would inhibit talin binding and so could indirectly impact filamin binding by reducing competition with talin. Hence, kinases may modulate integrin-filamin interactions either directly or indirectly.

Competition between Filamin and Talin

Multiple integrin-associated actin binding proteins have been identified, and the specific protein bound to the integrin tail has significant functional consequences. We and others have identified key roles for talin-integrin interactions, notably in integrin activation (Tadokoro et al., 2003) and during initial assembly of adhesive complexes and links to F-actin (Brown et al., 2002; Jiang et al., 2003). Characterization of the mechanisms regulating talin-integrin interactions has therefore become an important area of investigation. Our analysis of the FLNa-integrin complex revealed overlap with the talin binding site and competition between FLNa and talin for binding to integrin tails. Furthermore, in cells lacking FLNa, integrins are more active, consistent with increased talin binding due to release of a filamin-mediated inhibition.

This suggests that at least in certain circumstances, competition between filamin and talin can modulate talin-dependent processes.

Despite its requirement during integrin activation, talin binding is apparently not necessary during subsequent integrin-mediated outside-in signaling and cell spreading (Giannone et al., 2003; Arias-Salgado et al., 2005), when filamin may have a role (Glogauer et al., 1998; Calderwood et al., 2001). Thus, competition between filamin and talin may allow reorganization of integrin-links to F-actin or recruitment of specific populations of signaling molecules at different times or at different sites in the cell.

Competition may be modulated by integrin phosphorylation. As described above, filamin binding to integrin β tails may be inhibited by threonine phosphorylation, whereas talin binding is unaffected. Alternatively, although tyrosine phosphorylation of the NPxY motif inhibits talin binding (Garcia-Alvarez et al., 2003), its impact on filamin binding is unknown. This modulation could provide an additional tier of control on top of the signals from pathways directly acting on talin or filamin to determine their affinity for integrins (Calderwood, 2004). In this regard, it is noteworthy that T cell receptor complex activation can induce threonine phosphorylation of β7 integrins and increase β7-mediated adhesion (Hilden et al., 2003). It is tempting to speculate that by altering the balance between FLNa and talin binding to integrin β tails, kinases or phosphatases may modulate processes such as integrin activation and cell migration. However, it should be noted that many integrin β tail binding proteins have been identified (Liu et al., 2000), and many of these may also compete with either filamin or talin, or both filamin and talin, thus impacting integrin function. Hence, a complete characterization of this complex system will require additional information about the many proteins present at adhesion sites.

Deciphering the complex interplay between the multiple β tail binding proteins that connect integrins to the cytoskeleton and signaling networks, how their interactions are temporally and spatially regulated, and how this controls integrin activation, signalling, and cell migration remains a major challenge. The structure of an integrin-filamin complex described here provides detailed information on one interaction important in cell migration, reveals competition between filamin and talin for binding to integrin β tails, and suggests that phosphorylation of the β tail may allow selective dynamic regulation of these interactions.

Experimental Procedures

All antibodies were purchased from commercial suppliers as follows: polyclonal anti-GST (Chemicon), polyclonal anti-GFP (Rockland), monoclonal anti-talin (Sigma), and monoclonal anti-filamin MCA464S (Serotec) and mAb1680 (Chemicon). The epitope for MCA464S maps to the N-terminal 190 kDa fragment of filamin (Serotec), whereas the mAb1680 epitope maps to IgFLNa16–18 (our unpublished data). Bacterial expression constructs encoding recombinant His-tagged integrin cytoplasmic tail model proteins and GST-talin1 309–405 were produced and purified as previously described (Pfaff et al., 1998; Calderwood et al., 2001; Tadokoro et al., 2003). IgFLNa16-19 (amino acids 1765–2134), 19–21 (amino acids 2045–2329), 20–24 (amino acids 2135–2647), 19 (amino acids 2046–2141), 20 (amino acids 2142–2235), 21 (amino acids 2236–2329), 22 (amino acids 2326–2420), and 23 (amino acids 2421–2522) were generated by polymerase chain reaction (PCR) and subcloned into pGEX (Amersham) or EGFP (BD Biosciences) vectors for expression of GST- or EGFP-fusion proteins. Point mutations and deletions were introduced by QuikChange site-directed mutagenesis (Stratagene). The DNA sequence of all inserts was verified by sequencing. GST-fusion proteins were produced in *Escherichia coli* BL21 cells and purified on Glutathione Sepharose 4 Fast Flow medium (Amersham Biosciences) according to the manufacturer's instructions.

Binding assays with recombinant integrin tail model proteins were performed as previously described (Pfaff et al., 1998; Calderwood et al., 2001). For EGFP-fusion proteins or full-length human FLNa or FLNa mutants, Chinese hamster ovary (CHO) cells were transiently transfected with 3 μg of expression vector by using LipofectAMINE (Invitrogen). Cells were harvested 24–48 hr later, lysed as described previously (Calderwood et al., 2001), and binding assays were performed.

Stable FLNa knockdown lines in NIH 3T3 fibroblasts were generated with mFLNa shRNA vectors (OpenBiosystems). FLNa levels in all lines were assessed by immunoblotting. Integrin activation in NIH 3T3 FLNa knockdown lines was assessed by measuring binding of the fibronectin fragment FN9-11 by flow cytometry as previously described (Tadokoro et al., 2003).

For crystallography, DNA encoding human IgFLNa21 was cloned into a modified pGEX4T-3 plasmid encoding the Tobacco etch virus (TEV) protease cleavage site after the GST and thrombin recognition sequence. Protein was produced in BL21 cells, and cells were disrupted in PBS by using a French press. The soluble proteins were separated by ultracentrifugation at 150,000 × g for 30 min at 5ºC. The fusion protein was batch purified with Glutathione Sepharose 4 Fast Flow medium. After overnight cleavage with the TEV protease at 20ºC, the GST was separated from IgFLNa21 by Superdex 75 16/60 HR gel filtration (Amersham Biosciences) in 20 mM Tris-HCl (pH 8.0). Purified protein was concentrated with a YM-3000 centrifugal filter (Amicon) to 43.5 mg/ml, flash frozen in liquid nitrogen, and stored at −70ºC.

IgFLNa21 and the synthetic integrin β7 cytoplasmic tail peptide L^{768}NWKQDSNPLYKSAITTTINPRFQEADSPTL^{798} (numbering according to NCBI accession NM_000889.1) were cocrystallized by using the hanging drop vapor diffusion method. A solution containing equimolar concentrations (0.8 mM) of the protein in 20 mM Tris-HCl (pH 8.0) and the peptide in 50 mM Tris-HCl and 100 mM NaCl (pH 8.0) was mixed with the reservoir solution in a 1:1 ratio, and the crystals were grown in 1.26 M sodium citrate in 0.1 M citric acid (pH 5.5) at 22ºC. Prior to flash freezing in liquid nitrogen, the crystals were transferred through a series of solutions that gradually increased in glycerol content from 5% to 19%–20% in 1.28–1.29 M sodium citrate and 0.1 M citric acid (pH 5.5). Datasets were collected at 100 K at European Synchrotron Radiation Facility (Grenoble, France) beam lines ID23-1 (dataset fia1 wavelength 0.9795 Å) and ID14-3 (dataset fia5, 0.931 Å) by using MarMosaic 225 CCD and MARCCD detectors. The data were processed with the XDS program package (Kabsch, 1993).

The structure was determined with the programs in CCP4 suite from the graphical user interface (Potterton et al., 2003). The fia1 dataset was used for the structure determination by molecular replacement method with the program Phaser (Storoni et al., 2004) by using the polyalanine model of FLNc repeat 24 as a search model (Protein Data Bank [PDB] entry 1V05). After the density modification with DM (Cowtan, 1994), several rounds of manual model building with O (Jones et al., 1991) and restrained refinement applying NCS were performed. The polyalanine model of the partial structure containing two molecules in the asymmetric unit was then used as a search model in the molecular replacement of the fia5 dataset with Phaser. After rigid-body refinement with Refmac 5.2 (Murshudov et al., 1997), the model was used as an input for 20 cycles of automated model building by using the warpNtrace procedure (Perrakis et al., 1999). ARP/wARP solvent atom and automated ligand building procedures (Perrakis et al., 1999) were used when adding water and glycerol molecules, respectively. The final model was built manually with O and refined by using Refmac 5.2, applying TLS and restraint refinement. The electrostatic potential surface of the IgFLNa21 was calculated with Grasp (Nicholls et al., 1991) (http://trantor.bioc.columbia.edu/grasp/), and the images were generated with PyMol

(DeLano Scientific, San Carlos, CA, USA; http://www.pymol.org). In the final model, 95.2% of residues were in the most favored regions of the Ramachandran plot and 4.8% were in the additionally allowed regions.

For NMR experiments, wild-type IgFLNa21 and 19 were produced as for the crystallography experiments. The $C^{2293}S$ IgFLNa21 mutant was produced and purified by using previously described methods (de Pereda et al., 2005). The identity and purity of the final protein was confirmed by electrospray mass spectrometry and sodium dodecyl-sulfate-polyacrylamide gel electrophoresis (SDS-PAGE). The β7 integrin peptide N^{775}PLYKSAITTTINPRF^{790} (N-terminally acetylated and C-terminally amidated) and the β3 integrin peptide K^{738}WDTANNPLYKEATSTFTNITYRGT^{762} (N-terminally acetylated) were purchased from Alta Bioscience (Birmingham, UK) and were further purified by reverse-phase high performance liquid chromatography.

All NMR experiments were carried out by using previously described methods (de Pereda et al., 2005). The backbone amide ^{15}N and ^{1}H shifts of each protein domain studied were assigned by using samples of 1.4 mM U-^{15}N-labeled IgFLNa21, 1.0 mM U-^{15}N-labeled IgFLNa21($C^{2293}S$), and 1.0 mM U-^{15}N-labeled IgFLNa19, each in 90% H_2O and 10% D_2O. All samples were buffered with 50 mM phosphate (pH 6.1) containing 100 mM NaCl. Wild-type protein samples also contained 10 mM DTT. Data processing was carried out with NMRPipe (Delaglio et al., 1995), and spectra were assigned by using the program SPARKY (www.cgl.ucsf.edu/home/sparky). Spectra were referenced to the water signal (4.766 ppm ^{1}H ref), with indirect referencing in the ^{15}N dimension by using a ^{15}N-^{1}H frequency ratio of 0.101329118. For each peptide binding titration, a sample containing 100 μM U-^{15}N-labeled filamin was added to increasing amounts of freeze-dried β integrin peptide, and two-dimensional gradient-enhanced ^{1}H-^{15}N HSQC spectra with water flip-back were acquired at each titration point (de Pereda et al., 2005). The concentrations of the β integrin peptides used in the titrations were typically 0, 10, 25, 50, 100, 150, 200, 300, 400, 600, 800, and 1000 μM.

Supplemental Data

Supplemental Data include one table and one figure and can be found with this article online at http://www.molecule.org/cgi/content/full/21/3/337/DC1/.

Acknowledgments

This work was supported by grants from the National Institutes of Health (RO1 GM068600-01), the American Heart Association (0230304N), and the Academy of Finland (51863, 202725, 203675). M.B. was supported by a fellowship from FIRC. We acknowledge the European Synchrotron Radiation Facility and thank Drs. Didier Nurizzio, Joanne McCarthy, and Chloé Zubieta for assistance in using beamlines ID23-1 and ID14-3.

Received: August 31, 2005
Revised: November 3, 2005
Accepted: January 4, 2006
Published: February 2, 2006

References

Arias-Salgado, E.G., Lizano, S., Shattil, S.J., and Ginsberg, M.H. (2005). Specification of the direction of adhesive signaling by the integrin β cytoplasmic domain. J. Biol. Chem. *280*, 29699–29707.

Ayed, A., Mulder, F.A., Yi, G.S., Lu, Y., Kay, L.E., and Arrowsmith, C.H. (2001). Latent and active p53 are identical in conformation. Nat. Struct. Biol. *8*, 756–760.

Brown, N.H., Gregory, S.L., Rickoll, W.L., Fessler, L.I., Prout, M., White, R.A., and Fristrom, J.W. (2002). Talin is essential for integrin function in Drosophila. Dev. Cell *3*, 569–579.

Calderwood, D.A. (2004). Integrin activation. J. Cell Sci. *117*, 657–666.

Calderwood, D.A., Huttenlocher, A., Kiosses, W.B., Rose, D.M., Woodside, D.G., Schwartz, M.A., and Ginsberg, M.H. (2001). Increased filamin binding to β-integrin cytoplasmic domains inhibits cell migration. Nat. Cell Biol. *3*, 1060–1068.

Cowtan, K. (1994). 'dm': An automated procedure for phase improvement by density modification. Joint CCP4 and ESF-EACBM Newsletter on Protein Crystallography *31*, 34–38.

Cunningham, C.C., Gorlin, J.B., Kwiatkowski, D.J., Hartwig, J.H., Janmey, P.A., Byers, H.R., and Stossel, T.P. (1992). Actin-binding protein requirement for cortical stability and efficient locomotion. Science *255*, 325–327.

de Pereda, J.M., Wegener, K.L., Santelli, E., Bate, N., Ginsberg, M.H., Critchley, D.R., Campbell, I.D., and Liddington, R.C. (2005). Structural basis for phosphatidylinositol phosphate kinase type Iγ binding to talin at focal adhesions. J. Biol. Chem. *280*, 8381–8386.

Delaglio, F., Grzesiek, S., Vuister, G.W., Zhu, G., Pfeifer, J., and Bax, A. (1995). NMRPipe: a multidimensional spectral processing system based on UNIX pipes. J. Biomol. NMR *6*, 277–293.

Fagerholm, S.C., Hilden, T.J., and Gahmberg, C.G. (2004). P marks the spot: site-specific integrin phosphorylation regulates molecular interactions. Trends Biochem. Sci. *29*, 504–512.

Feng, Y., and Walsh, C.A. (2004). The many faces of filamin: a versatile molecular scaffold for cell motility and signalling. Nat. Cell Biol. *6*, 1034–1038.

Flanagan, L.A., Chou, J., Falet, H., Neujahr, R., Hartwig, J.H., and Stossel, T.P. (2001). Filamin A, the Arp2/3 complex, and the morphology and function of cortical actin filaments in human melanoma cells. J. Cell Biol. *155*, 511–517.

Garcia-Alvarez, B., de Pereda, J.M., Calderwood, D.A., Ulmer, T.S., Critchley, D.R., Campbell, I.D., Ginsberg, M.H., and Liddington, R.C. (2003). Structural determinants of integrin recognition by talin. Mol. Cell *11*, 49–58.

Giannone, G., Jiang, G., Sutton, D.H., Critchley, D.R., and Sheetz, M.P. (2003). Talin1 is critical for force-dependent reinforcement of initial integrin-cytoskeleton bonds but not tyrosine kinase activation. J. Cell Biol. *163*, 409–419.

Glogauer, M., Arora, P., Chou, D., Janmey, P.A., Downey, G.P., and McCulloch, C.A. (1998). The role of actin-binding protein 280 in integrin-dependent mechanoprotection. J. Biol. Chem. *273*, 1689–1698.

Hilden, T.J., Valmu, L., Karkkainen, S., and Gahmberg, C.G. (2003). Threonine phosphorylation sites in the β2 and β7 leukocyte integrin polypeptides. J. Immunol. *170*, 4170–4177.

Hynes, R.O. (2002). Integrins: bidirectional, allosteric signaling machines. Cell *110*, 673–687.

Jiang, G., Giannone, G., Critchley, D.R., Fukumoto, E., and Sheetz, M.P. (2003). Two-piconewton slip bond between fibronectin and the cytoskeleton depends on talin. Nature *424*, 334–337.

Jones, T.A., Zou, J.Y., Cowan, S.W., and Kjeldgaard. (1991). Improved methods for building protein models in electron density maps and the location of errors in these models. Acta Crystallogr. A *47(Pt.2)*, 110–119.

Kabsch, W. (1993). Automatic processing of rotation diffraction data from crystals of initially unknown symmetry and cell constants. J. Appl. Crystallogr. *26*, 795–800.

Liu, S., Calderwood, D.A., and Ginsberg, M.H. (2000). Integrin cytoplasmic domain-binding proteins. J. Cell Sci. *113*, 3563–3571.

McCoy, A.J., Fucini, P., Noegel, A.A., and Stewart, M. (1999). Structural basis for dimerization of the Dictyostelium gelation factor (ABP120) rod. Nat. Struct. Biol. *6*, 836–841.

Murshudov, G.N., Vagin, A.A., and Dodson, E.J. (1997). Refinement of macromolecular structures by the maximum-likelihood method. Acta Crystallogr. D Biol. Crystallogr. *53*, 240–255.

Nagano, T., Yoneda, T., Hatanaka, Y., Kubota, C., Murakami, F., and Sato, M. (2002). Filamin A-interacting protein (FILIP) regulates cortical cell migration out of the ventricular zone. Nat. Cell Biol. *4*, 495–501.

Nakamura, F., Pudas, R., Heikkinen, O., Permi, P., Kilpelainen, I., Munday, A.D., Hartwig, J.H., Stossel, T.P., and Ylanne, J. (2006). The structure of the GPIb-filamin A complex. Blood *107*, 1925–1932.

Nicholls, A., Sharp, K.A., and Honig, B. (1991). Protein folding and association: insights from the interfacial and thermodynamic properties of hydrocarbons. Proteins *11*, 281–296.

Perrakis, A., Morris, R., and Lamzin, V.S. (1999). Automated protein model building combined with iterative structure refinement. Nat. Struct. Biol. *6*, 458–463.

Pfaff, M., Liu, S., Erle, D.J., and Ginsberg, M.H. (1998). Integrin β cytoplasmic domains differentially bind to cytoskeletal proteins. J. Biol. Chem. *273*, 6104–6109.

Popowicz, G.M., Muller, R., Noegel, A.A., Schleicher, M., Huber, R., and Holak, T.A. (2004). Molecular structure of the rod domain of dictyostelium filamin. J. Mol. Biol. *342*, 1637–1646.

Potterton, E., Briggs, P., Turkenburg, M., and Dodson, E. (2003). A graphical user interface to the CCP4 program suite. Acta Crystallogr. D Biol. Crystallogr. *59*, 1131–1137.

Pudas, R., Kiema, T.R., Butler, P.J., Stewart, M., and Ylanne, J. (2005). Structural basis for vertebrate filamin dimerization. Structure (Camb.) *13*, 111–119.

Ridley, A.J., Schwartz, M.A., Burridge, K., Firtel, R.A., Ginsberg, M.H., Borisy, G., Parsons, J.T., and Horwitz, A.R. (2003). Cell migration: integrating signals from front to back. Science *302*, 1704–1709.

Sharma, C.P., Ezzell, R.M., and Arnaout, M.A. (1995). Direct interaction of filamin (ABP-280) with the β2-integrin subunit CD18. J. Immunol. *154*, 3461–3470.

Springer, T.A., and Wang, J.H. (2004). The three-dimensional structure of integrins and their ligands, and conformational regulation of cell adhesion. Adv. Protein Chem. *68*, 29–63.

Storoni, L.C., McCoy, A.J., and Read, R.J. (2004). Likelihood-enhanced fast rotation functions. Acta Crystallogr. D Biol. Crystallogr. *60*, 432–438.

Stossel, T.P., Condeelis, J., Cooley, L., Hartwig, J.H., Noegel, A., Schleicher, M., and Shapiro, S.S. (2001). Filamins as integrators of cell mechanics and signalling. Nat. Rev. Mol. Cell Biol. *2*, 138–145.

Tadokoro, S., Shattil, S.J., Eto, K., Tai, V., Liddington, R.C., de Pereda, J.M., Ginsberg, M.H., and Calderwood, D.A. (2003). Talin binding to integrin β tails: a final common step in integrin activation. Science *302*, 103–106.

Travis, M.A., van der Flier, A., Kammerer, R.A., Mould, A.P., Sonnenberg, A., and Humphries, M.J. (2004). Interaction of filamin A with the integrin β7 cytoplasmic domain: role of alternative splicing and phosphorylation. FEBS Lett. *569*, 185–190.

Ulmer, T.S., Calderwood, D.A., Ginsberg, M.H., and Campbell, I.D. (2003). Domain-specific interactions of talin with the membrane-proximal region of the integrin β3 subunit. Biochemistry *42*, 8307–8312.

van der Flier, A., and Sonnenberg, A. (2001). Structural and functional aspects of filamins. Biochim. Biophys. Acta *1538*, 99–117.

van der Flier, A., Kuikman, I., Kramer, D., Geerts, D., Kreft, M., Takafuta, T., Shapiro, S.S., and Sonnenberg, A. (2002). Different splice variants of filamin-B affect myogenesis, subcellular distribution, and determine binding to integrin β subunits. J. Cell Biol. *156*, 361–376.

Zent, R., Fenczik, C.A., Calderwood, D.A., Liu, S., Dellos, M., and Ginsberg, M.H. (2000). Class- and splice variant-specific association of CD98 with integrin β cytoplasmic domains. J. Biol. Chem. *275*, 5059–5064.

Accession Numbers

The atomic coordinates for the IgFLNa21-integrin β7 peptide complex have been deposited in the PDB with ID code 2BRQ.